Available online at www.sciencedirect.com
ScienceDirect
Mechanics of Materials 39 (2007) 212–221
MECHANICS OF MATERIALS
www.elsevier.com/locate/mechmat

Elastoplastic modelling of hydraulic and stress–strain behaviour of unsaturated soils

De'an Sun [a,*], Daichao Sheng [b], Scott W. Sloan [b]

[a] Department of Civil Engineering, Shanghai University, 149 Yanchang Road, Shanghai 200072, PR China
[b] Discipline of Civil, Surveying and Environmental Engineering, School of Engineering, University of Newcastle, NSW 2308, Australia

Received 9 September 2005

Abstract

This paper presents an elastoplastic model for predicting the hydraulic and stress–strain behaviour of unsaturated soils. The model takes into consideration the effect of the degree of saturation on stress–strain behaviour, the effect of the void ratio on water-retention behaviour, and the influence of suction. Model predictions of the stress–strain and water-retention response are compared with those obtained from triaxial tests on unsaturated soil during isotropic and shear loading with and without suction change. The comparisons indicate that the model can quantitatively reproduce the hydraulic and mechanical behaviour of unsaturated soils.

Keywords: Elastoplastic model; Unsaturated soil; Stress–strain behaviour; Water-retention behaviour; Triaxial test

1. Introduction

Starting with the model proposed by Alonso et al. (1990), several elastoplastic constitutive laws for unsaturated soils have been developed which are based on experimental and theoretical studies (Kohgo et al., 1993; Wheeler and Sivakumar, 1995; Sun et al., 2000). The stress-state variables employed in most models for unsaturated soils are the net stress (the difference between total stress and pore-air pressure) and the suction (the difference between pore-air pressure and pore-water pressure). In the earliest models the unsaturated states were expressed only in terms of the suction, with the degree of saturation being computed from the suction; so that hydraulic hysteresis was not incorporated. These models were also difficult to implement in existing finite element codes for saturated soils because most saturated soil relations are described in term of effective stress (Sheng et al., 2004). In recent years, some conceptual models incorporating hydraulic hysteresis of unsaturated soils have been proposed (Buisson and Wheeler, 2000; Vaunat et al., 2000; Gallipoli et al., 2003; Wheeler et al., 2003; Tamagnini, 2004; Sheng et al., 2004). However, most of these can describe the hydraulic and stress–strain behaviour only in qualitative terms, and are formulated only for isotropic stress conditions. The present paper gives a complete formulation of an elastoplastic model

* Corresponding author. Fax: +86 21 56331971.
E-mail address: sundean06@163.com (D. Sun).

0167-6636/$ - see front matter © 2006 Elsevier Ltd. All rights reserved.
doi:10.1016/j.mechmat.2006.05.002

Nomenclature

e	void ratio	u_w	pore-water pressure
f	yield function	$\varepsilon_v^e, \varepsilon_v^p$	elastic and plastic volumetric strains
g	plastic potential	κ	swelling index
M	slope of critical state line in q–p' plane	κ_s	slope of scanning curve in S_r–ln$s$ plot
p	mean net stress	$\lambda(0)$	value of $\lambda(s)$ at zero suction
p'	mean effective stress	$\lambda(s)$	slope of normal compression line in e–lnp' plot
p_a	atmospheric pressure		
p'_n	reference pressure	λ_s	parameter for identifying the change of $\lambda(s)$ with suction s
p'_y	'effective' yield stress		
p_{0y}	yield stress at zero suction	λ_{se}	slope of S_r versus e relation under constant suction
q	deviator stress		
s	suction	λ_{sr}	slope of main curves in S_r–ln$s$ plot under constant void ratio
S_r	degree of saturation		
u_a	pore-air pressure	σ'_{ij}	'effective' stress tensor

which incorporates the hydraulic and mechanical behaviour of unsaturated soils. The predictions of the model are validated quantitatively by experimental results obtained from suction-controlled triaxial tests on unsaturated soil.

The paper is organised as follows. First, experimental results for the void ratio versus the degree of saturation are presented—based on suction-controlled isotropic compression tests and triaxial compression tests on unsaturated compacted clay. Secondly, an elastoplastic model for unsaturated soils, which incorporates hydraulic behaviour, is formulated. Finally, the model predictions are compared with the experimental results for various loading paths and wetting paths.

2. Experimental study on water-retention behaviour

To investigate the influence of void ratio on water-retention behaviour, and to obtain the stress–strain relations under different initial degrees of saturation, a series of isotropic compression tests and triaxial compression tests on unsaturated compacted clay were performed using a suction-controlled triaxial apparatus. The soil used in this study is called 'Pearl clay'. It contains 50% silt and 50% clay, and has a liquid limit of 49% and a plasticity index of 22. There are few expansive clay minerals in Pearl clay. Triaxial specimens were prepared by compaction in a mould at a water content of about 26%. Specimens were compacted in five layers, and the initial void ratio and initial degree of saturation were controlled by changing the compaction energy. The triaxial apparatus can directly measure the lateral strain of the specimen, and can also control the matric suction. The lateral displacement of the specimen was measured using three rings made of stainless steel mounted at $H/4$, $H/2$ and H from the top of the specimen, with H being the specimen height (Sun et al., 2003, 2004). The specimen volume was calculated from the lateral displacements measured by the three rings, using the assumption that the lateral shape is approximated by a third-order polynomial. The pore-water pressure was maintained at atmospheric pressure during the constant suction and wetting tests through a ceramic disk installed in the pedestal with an air-entry value of 300 kPa. The pore-air pressure was applied at the top through a one-way filter that can prevent water from seeping out. Hence, the change in the water volume in the burette is the same as the change in the water volume of the tested specimen, thus allowing the degree of saturation to be calculated. For other details, see Sun et al. (2000, 2003, 2004). The imposed stress paths in each case can be varied, depending on the objective of each test. The detailed stress path of each particular test will be explained in the paper when the test results are described. To investigate the influence of void ratio on water-retention behaviour, two kinds of tests were performed under isotropic stress conditions—(i) the suction imposed on specimens with different initial void ratios was reduced under constant isotropic net stress; and (ii) the isotropic net stress imposed on specimens with different initial void ratios was increased under constant suction.

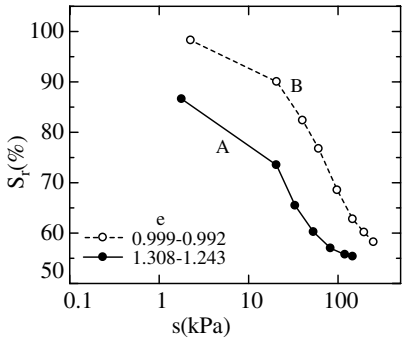

Fig. 1. Water retention curves for different void ratios during wetting.

Fig. 1 shows the water retention curves for unsaturated compacted specimens A and B with different initial void ratios, obtained from tests with constant isotropic net stresses. These specimens were first isotropically consolidated at a mean total stress p_t of 20 kPa. Differential air pressures were then applied to the specimens (147 kPa for A and 245 kPa for B) with a mean net stress p of 20 kPa (where the mean net stress $p = p_t - u_a$). The drainage valve was then opened to dissipate the pore-water pressure so that $u_w = 0$. Specimen A was then wetted by decreasing the imposed suction step by step, whereas specimen B was loaded to an isotropic net stress of 98 kPa under a constant suction of 245 kPa. To perform collapse tests, the imposed suction was decreased in a drained mode under constant net stress conditions. The range of e indicated in the figure is the change in the void ratio during the wetting tests. From other tests, it was known that the initial suctions of specimen A and B were about 100 and 200 kPa, respectively. The part of the curve with a suction larger than the initial suction represents the scanning curve, and the part of the curve with a suction smaller than the initial suction represents the main wetting curve. It can be seen that the main wetting curve is shifted to the right when the initial void ratio of the specimens decreases. This is because the decrease in the void ratio results in a decrease in connecting passageways between the voids, and hence an increase in the air-entry value (Ng and Pang, 2000).

Fig. 2 shows the experimental relation between the degree of saturation and the void ratio from triaxial tests and the corresponding stress paths during isotropic compression loading and/or shear loading under a constant suction of 147 kPa. These specimens were compacted at different initial void ratios

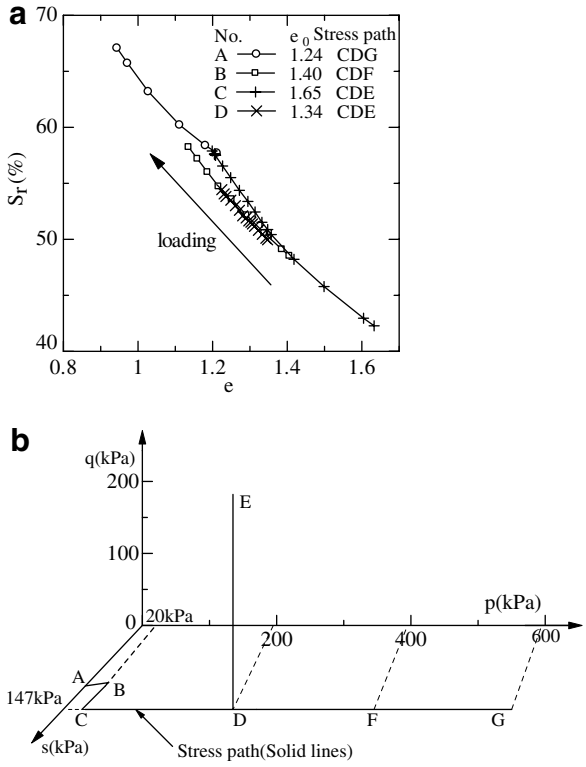

Fig. 2. Relation between void ratio and degree of saturation during isotropic loading and triaxial tests under $s = 147$ kPa: (a) relation between void ratio and degree of saturation, (b) imposed stress paths.

and different initial degrees of saturation, and were first isotropically consolidated at a mean total stress p_t of 20 kPa with an initial suction of about 100 kPa. An air pressure of 147 kPa was then applied to the specimens with a mean net stress p of 20 kPa. The drainage valve was again opened to zero the pore-water pressure, and the specimens were loaded isotropically to a net stress of 196 kPa or 392 kPa or 588 kPa, step by step, under a constant suction of 147 kPa. Specimens C and D were sheared to failure under $p = 196$ kPa and a suction $s = 147$ kPa. It can be seen that, even under the same imposed suction, the degree of saturation increases when the unsaturated specimens are compressed. It is interesting to note that the measured relations between the degree of saturation and the void ratio for specimens with different initial void ratios are very similar, and can be considered to be linear. This linear relation seems to be true both before and after yielding, because the initial yield stress, which depends on the initial density of the specimen, is inside the range of the isotropic

loading. Therefore, it can be introduced into the model in both the elastic and elastoplastic zones.

From Figs. 1 and 2, it can be concluded that the water-retention curve of unsaturated compacted clays is dependent not only on the wetting process (or the drying process), but also on the void ratio. Therefore, modelling of the water-retention curve of unsaturated compacted clays needs to take the void ratio into consideration. A good starting-point for modelling the water-retention curve is to assume that the degree of saturation S_r is linearly related to the logarithmic value of the suction $\ln s$ (Wheeler et al., 2003). In Fig. 3, the main drying and wetting curves have a gradient λ_{sr} and the scanning curves have a gradient κ_s. That is to say, the scanning curve and the main drying and wetting curves of the water-retention curve are described respectively by

$$S_r = S_r^0(e) - \kappa_s \ln \frac{s}{p_a} \tag{1}$$

and

$$S_r = S_r^0(e) - \lambda_{sr} \ln \frac{s}{p_a} \tag{2}$$

where $S_r^0(e)$ is the degree of saturation at $s = p_a$, and is a function of the void ratio e, and p_a is atmospheric pressure.

Taking in account the experimental results shown in Fig. 2, Eqs. (1) and (2) can be rewritten as

$$S_r = S_{r0} - \lambda_{se}(e - e_0) - \kappa_s \ln \frac{s}{p_a} \tag{3}$$

and

$$S_r = S_{r0} - \lambda_{se}(e - e_0) - \lambda_{sr} \ln \frac{s}{p_a} \tag{4}$$

where S_{r0} is the degree of saturation at $s = p_a$ and $e = e_0$, and λ_{se} is the gradient of the S_r versus e relation under constant suction. Differentiating Eqs. (3) and (4) gives:

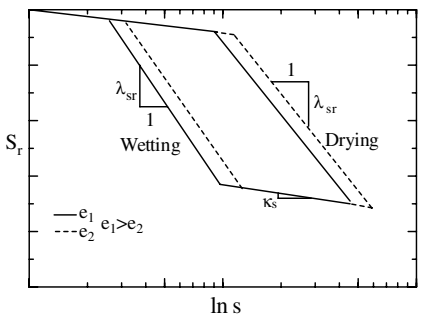

Fig. 3. Model for water retention behaviour at different void ratios.

$$dS_r = -\lambda_{se}\, de - \kappa_s \frac{ds}{s} \tag{5}$$

and

$$dS_r = -\lambda_{se}\, de - \lambda_{sr} \frac{ds}{s} \tag{6}$$

3. Elastoplastic model incorporating water-retention behaviour

This paper presents an elastoplastic constitutive model for unsaturated soils, incorporating the influence of the degree of saturation on the stress–strain relation and strength, and the influence of deformation on water-retention behaviour. The model is applicable to unsaturated soils in which pore air and pore water are continuous throughout the voids.

3.1. Stress-state variable for unsaturated soil

To identify the hydraulic and mechanical behaviour of unsaturated soils properly, the stress-state variables employed in the model are the 'effective stress' tensor σ'_{ij} and the suction s, and the strain-state variables are the soil skeleton strain tensor ε_{ij} and the degree of saturation S_r. The 'effective stress' tensor σ'_{ij} is defined by

$$\sigma'_{ij} = \sigma_{ij} - u_a \delta_{ij} + S_r s \delta_{ij} \tag{7}$$

where σ_{ij} is the total stress tensor, S_r is the saturation degree, u_a is the pore-air pressure, and δ_{ij} is the Kronecker delta. Eq. (7) is similar to the effective stress proposed by Bishop and Blight (1963), with S_r taking the place of the weighting factor χ. Note that Lewis and Schrefler (1987) first used S_r as the effective stress parameter for unsaturated soils. The 'effective stress' automatically becomes Terzaghi's effective stress for the saturated state. The 'effective stress' is the same as the 'average stress' (Jommi, 2000), or 'Bishop's stress' (Wheeler et al., 2003), or the 'constitutive stress' (Sheng et al., 2004). The 'effective stress' and the suction are not independent variables, but their work-conjugate strains (soil skeleton strains and the degree of saturation) are independent variables (Sheng et al., 2004). In previous work the so-called translated stress and suction have been used as the stress-state variables for modelling the mechanical behaviour of unsaturated soil (Sun et al., 2000, 2003). The 'effective stress' and suction variables adopted in the present study permit a general form of hydraulic

behaviour to be represented and also provide a smooth transition between the saturated and unsaturated states.

3.2. Formulation of the constitutive model for isotropic stress states

In previous work, one of the present authors developed a so-called 'load-collapse' (LC) yield curve in the p-s plane under an isotropic stress state (Sun et al., 2000). A similar form is adopted in the following equation, except that the 'effective stress' is newly defined as per Eq. (7).

$$p'_y = p'_n \left(\frac{p_{0y}}{p'_n}\right)^{\frac{\lambda(0)-\kappa}{\lambda(s)-\kappa}} \tag{8}$$

or

$$p_{0y} = p'_n \left(\frac{p'_y}{p'_n}\right)^{\frac{\lambda(s)-\kappa}{\lambda(0)-\kappa}} \tag{9}$$

where p_{0y} and p'_y are the 'effective' yield stresses for saturated soil and unsaturated soil with suction s (see Fig. 4); p'_n is an isotropic stress at which no collapse occurs when the suction is decreased; κ is a swelling index for unsaturated soils (including saturated soil in the e–$\ln p'$ plane); and $\lambda(0)$ and $\lambda(s)$ are the slopes of the normal compression lines of saturated soil and unsaturated soil with suction s in the e–$\ln p'$ plane. The quantity $\lambda(s)$ is assumed as per Sun et al. (2000):

$$\lambda(s) = \lambda(0) + \frac{\lambda_s s}{p_a + s} \tag{10}$$

where λ_s is a material parameter for identifying the change of $\lambda(s)$ with suction s.

From Eq. (8) we have

$$\mathrm{d}p'_y = \frac{\partial p'_y}{\partial p_{0y}}\,\mathrm{d}p_{0y} + \frac{\partial p'_y}{\partial s}\,\mathrm{d}s \tag{11}$$

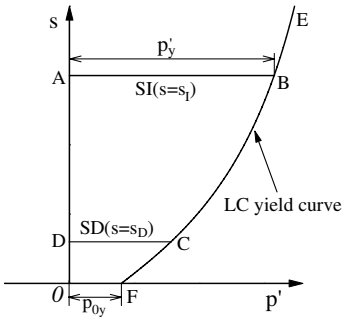

Fig. 4. LC yield curve, SI and SD yield curves for isotropic stress states.

where

$$\frac{\partial p'_y}{\partial p_{0y}} = \frac{\lambda(0)-\kappa}{\lambda(s)-\kappa}\left(\frac{p_{0y}}{p'_n}\right)^{\frac{\lambda(0)-\lambda(s)}{\lambda(s)-\kappa}} \tag{12}$$

$$\frac{\partial p'_y}{\partial s} = \frac{\lambda_s p'_n p_a (\lambda(0)-\kappa)}{(\lambda(s)-\kappa)^2}\ln\left(\frac{p'_n}{p_{0y}}\right)\left(\frac{1}{p_a+s}\right)^2\left(\frac{p_{0y}}{p'_n}\right)^{(\lambda(0)-\kappa)/(\lambda(s)-\kappa)} = \frac{\lambda_s p'_y p_a (\lambda(0)-\kappa)}{(\lambda(s)-\kappa)^2 (p_a+s)^2}\ln\left(\frac{p'_n}{p_{0y}}\right) \tag{13}$$

When the stress state is inside the LC yield curve, the elastic volumetric strain increment is given by

$$\mathrm{d}\varepsilon_v^e = \frac{\kappa\,\mathrm{d}p'}{(1+e)p'} \tag{14}$$

When the stress state is on the LC yield curve, the plastic volumetric strain increment is given by

$$\mathrm{d}\varepsilon_v^p = \frac{(\lambda(0)-\kappa)\,\mathrm{d}p_{0y}}{(1+e)p_{0y}} \tag{15}$$

or, from Eq. (11):

$$\mathrm{d}\varepsilon_v^p = \frac{\lambda(0)-\kappa}{(1+e)p_{0y}}\left(\mathrm{d}p'_y - \frac{\partial p'}{\partial s}\,\mathrm{d}s\right)\Big/\frac{\partial p'}{\partial p_{0y}} \tag{16}$$

In addition to the LC yield curve, two more yield curves are needed to model hydraulic hysteresis as an elastoplastic process, as shown in Fig. 4. The water-retention behaviour shown in Fig. 3 is represented by a suction increase (SI) yield curve and a suction decrease (SD) yield curve in the $p' - s$ plane. When the suction changes during a drying ($s \geqslant s_I$) or wetting ($s \leqslant s_D$) process, the degree of saturation increment is given by Eq. (6); otherwise, the degree of saturation increment given by Eq. (5). Therefore, according to the relation between the stress state (p' and s) and the yield curves (LC, SI, and SD), different equations must be used to calculate the strains and the degree of saturation. When $\mathrm{d}p_{0y} > 0$ and $s > s_I$ or $s < s_D$, the volumetric strains and the degree of saturation are calculated by Eqs. (14), (15) and (6). When $\mathrm{d}p_{0y} > 0$ and $s_D \leqslant s \leqslant s_I$, they are calculated by Eqs. (14), (15) and (5). When $\mathrm{d}p_{0y} < 0$, and $s > s_I$ or $s < s_D$, the volumetric strain and the degree of saturation are calculated by Eqs. (14) and (6). When $\mathrm{d}p_{0y} < 0$ and $s_D \leqslant s \leqslant s_I$, they are calculated by Eqs. (14) and (5).

3.3. Formulation of the constitutive model under axisymmetric stress states

The Modified Cam-clay model has been used extensively for saturated soils, and gives reasonably

good predictions for clays. This model is adopted here because it is simple and all its parameters have clear physical meanings. Assuming an associated flow rule, the yield function (f) and the plastic potential function (g) are proposed to have the following form:

$$f = g = q^2 + M^2 p'(p' - p'_y) = 0 \tag{17}$$

Fig. 5 shows the geometrical shape of the yield function for $s > 0$ (unsaturated state) and $s = 0$ (saturated state).

The associated flow rule is obeyed in the 'effective stress' space; that is

$$d\varepsilon^p_{ij} = \Lambda \frac{\partial f}{\partial \sigma'_{ij}} \tag{18}$$

where the proportionality constant Λ can be determined from the consistency condition. Eq. (17) can be rewritten as $f = f(p', q, p'_y) = 0$, leading to:

$$df = \frac{\partial f}{\partial p'}dp' + \frac{\partial f}{\partial q}dq + \frac{\partial f}{\partial p'_y}dp'_y = 0 \tag{19}$$

Substituting Eq. (11) into Eq. (19) and re-arranging gives:

$$df = \frac{\partial f}{\partial p'}dp' + \frac{\partial f}{\partial q}dq + \frac{\partial f}{\partial p'_y}\frac{\partial p'_y}{\partial p_{0y}}dp_{0y} + \frac{\partial f}{\partial p'_y}\frac{\partial p'_y}{\partial s}ds = 0 \tag{20}$$

where the isotropic yielding stress p_{0y} for saturated soil is related to the volumetric strain ε^p_v and is the same as that used in the traditional Cam-clay model. Because the plastic volumetric strain ε^p_v is a hardening parameter in the present model, the volumetric plastic strains $d\varepsilon^p_v$ caused by dp_{0y} in a saturated soil are the same as those in an unsaturated soil which are caused by dp'_y and/or ds. Allowing for Eqs. (15) and (18), the following is obtained:

$$dp_{0y} = \frac{1+e}{\lambda(0)-\kappa}p_{0y}d\varepsilon^p_v = \frac{1+e}{\lambda(0)-\kappa}p_{0y}\Lambda\frac{\partial f}{\partial p'} \tag{21}$$

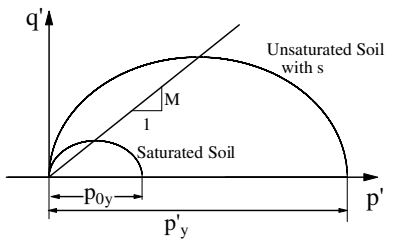

Fig. 5. Yield curves under constant suction.

Substituting Eq. (21) into Eq. (20) and solving for Λ gives:

$$\Lambda = -\frac{\frac{\partial f}{\partial p'}dp' + \frac{\partial f}{\partial q}dq + \frac{\partial f}{\partial p'_y}\frac{\partial p'_y}{\partial s}ds}{\frac{\partial f}{\partial p'_y}\frac{\partial p'_y}{\partial p_{0y}}p_{0y}\frac{1+e}{\lambda(0)-\kappa}\frac{\partial f}{\partial p'}} \tag{22}$$

in which:

$$\frac{\partial f}{\partial p'} = M^2(2p' - p_y) \tag{23}$$

$$\frac{\partial f}{\partial q} = 2q \tag{24}$$

$$\frac{\partial f}{\partial p'_y} = -M^2 p' \tag{25}$$

From Eqs. (18) and (22), it is possible to calculate the plastic strain increments caused by the increment in the 'effective stress' and/or the decrement in suction. The derivatives $\partial f/\partial p'$, $\partial f/\partial q$, and $\partial f/\partial p'_y$ are given in Eqs. (23)–(25), with $\partial p'_y/\partial p_{0y}$ and $\partial p'_y/\partial s$ being given in Eqs. (12) and (13).

4. Comparison of model predictions with experimental results

4.1. Model parameters and their determination

Because the proposed constitutive model is formulated within an elastoplastic framework, the strains consist of elastic and plastic components. The model requires five parameters to describe the stress–strain behaviour ($\lambda(0)$, λ_s, κ, p'_n and M) and three parameters to describe the water-retention behaviour (λ_{sr}, κ_s and λ_{se}).

To calculate the plastic strain, it is necessary to determine the model parameters $\lambda(0)$, λ_s, κ, p'_n and M. These model parameters are determined from the results of isotropic compression tests with wetting and loading–unloading–reloading processes, followed by subsequent triaxial compression tests on saturated and unsaturated soil under constant suction and constant p (or constant confining net stress).

Two tests are required to determine the model parameters. First, an isotropic compression test is conducted on unsaturated soil under a constant suction. Secondly, an unsaturated soil specimen is loaded to a small net stress (for example, $p =$ 50 kPa), and is then wetted to a saturated state. An isotropic compression test (with a loading–unloading–reloading cycle and a subsequent triaxial compression test) is then conducted on this

saturated specimen. From the result of the triaxial test on the saturated specimen, the internal friction angle (ϕ or M) can be determined. From the result of the isotropic compression test on the saturated specimen with a loading–unloading–reloading stress path, $\lambda(0)$ and κ can be determined. The quantity p'_n can be determined from the coordinates of the point where the two isotropic compression lines for the saturated and unsaturated specimens intersect. λ_s can be found from the values of $\lambda(0)$ and the compression index of the unsaturated specimen with suction s (using Eq. (10)).

The model parameters λ_{sr}, κ_s and λ_{se} define the water-retention curve and can be found as follows: λ_{se} is the slope of the $e - S_r$ line under constant suction, so λ_{se} can be determined by plotting e against S_r for an isotropic compression test on unsaturated soil under a constant suction. Thereafter, κ_s and λ_{sr} are determined from the results of a wetting test at small net stress by using Eqs. (3) and (4), or Eqs. (5) and (6).

The elastic component is calculated from Hooke's law, with Poisson's ratio assumed to be 1/3. The elastic modulus is calculated in the same way as for the Cam-clay model:

$$E = \frac{p'(1+e)}{\kappa} \tag{26}$$

The values of the relevant model parameters used in predicting the stress–strain and water-retention behaviour of the Pearl clay are as follows:

$$\lambda(0) = 0.12, \quad \kappa = 0.03, \quad \lambda_s = 0.12,$$
$$p'_n = 2\text{MPa}, \quad M = 1.1 \text{ and } \lambda_{se} = 0.35,$$
$$\lambda_{sr} = 0.13, \quad \kappa_s = 0.01$$

The model parameters for predicting the stress–strain behaviour are the same as those used previously by Sun et al. (2003), while the model parameters for predicting the water-retention curve were determined from Figs. 1 and 2.

4.2. Model prediction versus experimental results

Details of the clay properties, specimen preparation, triaxial apparatus, and testing procedure can be found in previous work of Sun et al. (2000, 2003, 2004). These studies provide information about the stress–strain behaviour of the soil; but do not give details of the measured water-retention behaviour. These are discussed below.

The stress paths in the following predictions of the test results were specified in terms of net stress $(\sigma_{ij} - u_a\delta_{ij})$ and suction s. Increments in σ'_{ij} are given by differentiating Eq. (7) according to

$$\mathrm{d}\sigma'_{ij} = \mathrm{d}(\sigma_{ij} - u_a\delta_{ij}) + (S_r\,\mathrm{d}s + s\,\mathrm{d}S_r)\delta_{ij} \tag{27}$$

Substituting Eqs. (5) and (6) into Eq. (27) gives:

$$\mathrm{d}\sigma'_{ij} = \mathrm{d}(\sigma_{ij} - u_a\delta_{ij}) + ((S_r - \kappa_s)\,\mathrm{d}s - \lambda_{se}s\mathrm{d}e)\delta_{ij} \tag{28}$$

$$\mathrm{d}\sigma'_{ij} = \mathrm{d}(\sigma_{ij} - u_a\delta_{ij}) + ((S_r - \lambda_{sr})\,\mathrm{d}s - \lambda_{se}s\mathrm{d}e)\delta_{ij} \tag{29}$$

Because Eqs. (28) and (29) involve de, this must be solved simultaneously with a constitutive model equation before the stress path can be defined in terms of the stress-state variables (the 'effective stress' tensor σ'_{ij} and the suction s).

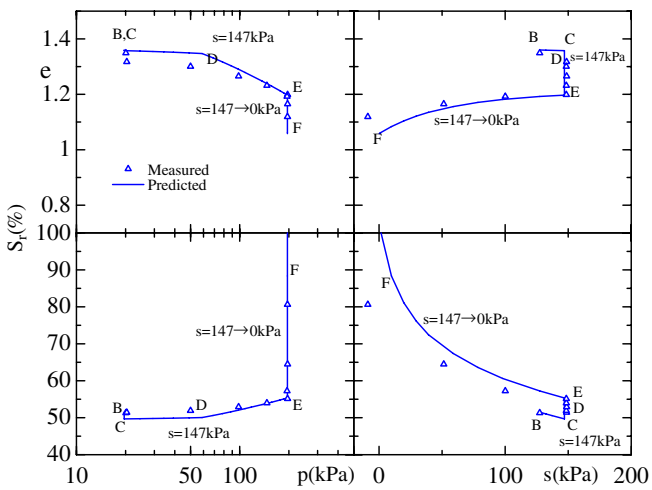

Fig. 6. Predicted and measured results of isotropic compression and wetting tests on unsaturated Pearl-clay.

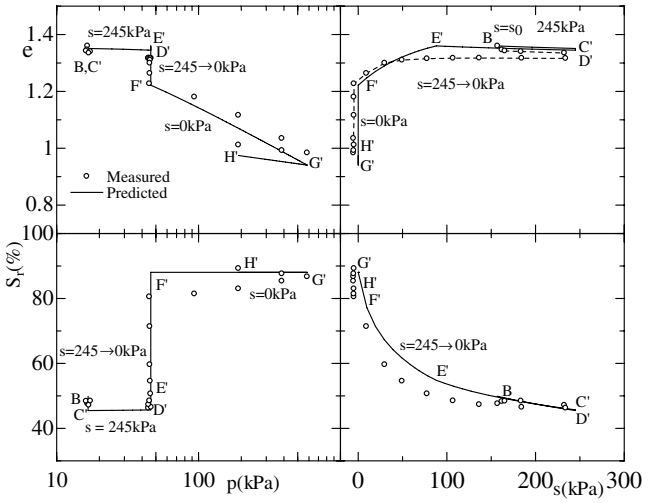

Fig. 7. Predicted and measured results of isotropic compression test ($s = 245$ kPa), wetting test ($s = 245 \rightarrow 0$ kPa) and isotropic compression test on Pearl-clay.

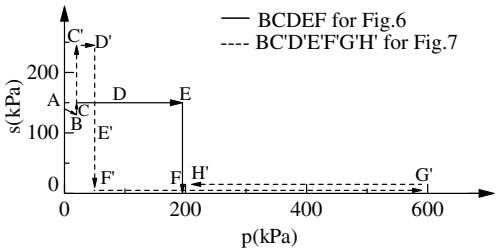

Fig. 8. Stress paths of isotropic loading tests.

Figs. 6 and 7 show comparisons between the predicted and measured results of the isotropic compression test and wetting test on unsaturated compacted Pearl clay. The stress paths imposed on the two specimens are shown in Fig 8—in which point A is the initial state of the specimens and p is a mean net stress. In addition to the above-mentioned model parameters, the initial state values—including initial net stress state (p_0), initial suction (s_0), initial void ratio (e_0), and initial yield stress p_{0y}—are needed in the model predictions. Values of $p_0 = 20$ kPa, $s_0 = 140$ kPa, $e_0 = 1.38$, and $p_{0y} = 15$ kPa were used in the model predictions in Figs. 6 and 7. It can be seen that the proposed model provides good predictions of the stress–strain and water-retention behaviour of unsaturated compacted clay. The predictions are accurate under constant suction and also during a wetting path under an isotropic stress state.

Fig. 9 shows a comparison of the predicted and measured results of triaxial compression tests on unsaturated compacted Pearl clay under constant mean net stress ($p = 196$ kPa) and constant suction

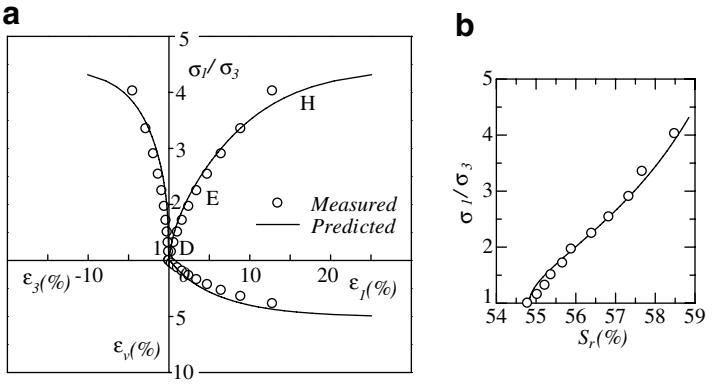

Fig. 9. Predicted and measured results of triaxial compression test on unsaturated Pearl-clay under $s = 147$ kPa and $p = 196$ kPa.

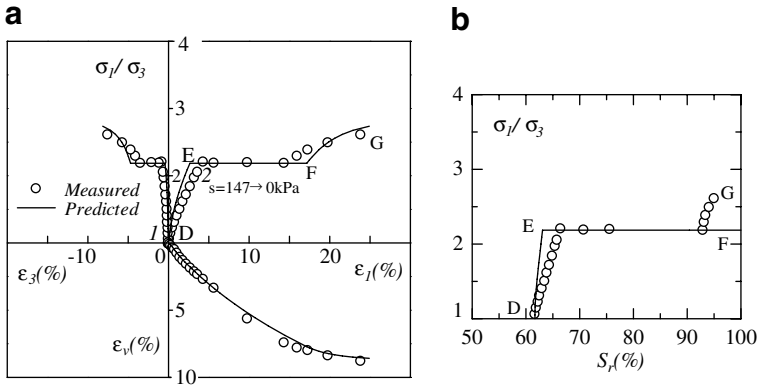

Fig. 10. Predicted and measured results of triaxial compression test under $s = 147$ kPa, wetting test ($s = 147 \rightarrow 0$ kPa) and triaxial compression test under $s = 0$ kPa ($p = 196$ kPa).

($s = 147$ kPa). Fig. 10 shows a comparison of the predicted and measured results of triaxial compression tests on unsaturated compacted Pearl clay under constant mean net or effective stress ($p = 196$ kPa), in which a wetting path ($s = 147$ kPa $\rightarrow 0$ kPa) was imposed with a stress ratio (σ_1/σ_3) of about 2.2 during shearing. The stress paths imposed on two specimens in Figs. 9 and 10 are shown in Fig. 11—path DEH for Fig. 9 and path DEFG for Fig. 10. It can be seen from Fig. 9 that the proposed model provides a good description of the stress–strain and water-retention behaviour of unsaturated compacted clay under constant suction during shearing. From Fig. 10, it can be seen that the proposed model provides an accurate description of the stress–strain and water-retention behaviour of unsaturated compacted clay—not only under constant suction but also under a wetting path. It is interesting to note that the model can provide a good prediction of the stress–strain-volume-change behaviour and the water-retention behaviour of unsaturated compacted soil during the processes of constant suction (D → H in Fig. 9 or Fig. 11, and D → E in Fig. 10 or Fig. 11), during suction reduction (E → F in Fig. 10 or Fig. 11), and during zero suction (F → G in Fig. 10 or Fig. 11) under triaxial compression stress.

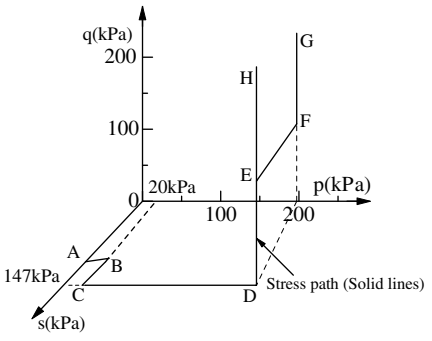

Fig. 11. Stress paths for triaxial test under $p = 196$ kPa.

It can be concluded from Figs. 6, 7, 9 and 10 that the proposed eight-parameter model is capable of providing good predictions of the stress–strain and water-retention behaviour (including collapse behaviour) of unsaturated compacted soil under isotropic or general stress paths. The model parameters can be determined from isotropic compression tests and triaxial compression tests on two unsaturated specimens with suction control.

5. Conclusions

(1) An elastoplastic constitutive model for unsaturated soils incorporating water-retention behaviour was proposed using a defined 'effective stress' tensor and the suction as stress-state variables. The effects of the suction and the degree of saturation on the stress–strain behaviour, and the effects of suction and the void ratio on water retention, have been taken into account in the model.

(2) Several isotropic compression and triaxial compression tests were carried out on unsaturated compacted clay using a suction-controlled triaxial apparatus. During the tests, the degree of saturation, the stresses, and the strains were measured under suction control. In particular, the wetting-induced collapse tests, under isotropic or anisotropic stress states, were performed by reducing the imposed suction.

(3) The model predicts the stress–strain-strength behaviour and the water-retention behaviour of the compacted clay along paths of constant suction or constant net stress. There are only eight model parameters, and these can be determined from isotropic compression tests and triaxial tests on two unsaturated specimens with suction control.

Acknowledgements

The authors wish to thank Professor Hajime Matsuoka of Nagoya Institute of Technology, Japan, for his useful comments. The first-named author acknowledges a visiting research grant provided by the University of Newcastle, Australia.

References

Alonso, F.E., Gens, A., Josa, A., 1990. A constitutive model for partially saturated soils. Geotechnique 40 (3), 405–430.

Bishop, A.W., Blight, G.E., 1963. Some aspects of effective stress in saturated and partly saturated soils. Geotechnique 13 (3), 177–197.

Buisson, M.S.R., Wheeler, S.J., 2000. Inclusion of hydraulic hysteresis in a new elastoplastic framework for unsaturated soils. In: Tarantino, A., Mancuso, C. (Eds.), Experimental Evidence and Theoretical Approaches in Unsaturated Soils, pp. 109–119.

Gallipoli, D., Gens, A., Sharma, R., Vaunat, J., 2003. An elastoplastic model for unsaturated soil incorporating the effects of suction and degree of saturation on mechanical behaviour. Geotechnique 53 (1), 123–135.

Jommi, C., 2000. Remarks on the constitutive modelling of unsaturated soils. In: Tarantino, A., Mancuso, C. (Eds.), Experimental Evidence and Theoretical Approaches in Unsaturated Soils, pp. 139–153.

Kohgo, Y., Nakano, M., Miyazaki, T., 1993. Theoretical aspects of constitutive modelling for unsaturated soils. Soils and Foundations 33 (4), 49–63.

Lewis, R.W., Schrefler, B.A., 1987. The Finite Element Method in the Static and Dynamic Deformation and Consolidation of Porous Media. Wiley and Sons, Chichester.

Ng, C.W.W., Pang, Y.W., 2000. Influence of stress state on soil-water characteristics and slope stability. ASCE Journal of Geotechnical and Geoenvironmental Engineering 126 (2), 157–166.

Sheng, D.C., Sloan, S.W., Gens, A., 2004. A constitutive model for unsaturated soils: thermomechanical and algorithmic aspects. Computational Mechanics 33, 453–465.

Sun, D.A., Matsuoka, H., Cui, H.B., Xu, X.F., 2003. Three-dimensional elastoplastic model for unsaturated compacted soils with different initial densities. International Journal for Numerical and Analytical Methods in Geomechanics 27, 1079–1098.

Sun, D.A., Matsuoka, H., Xu, Y.F., 2004. Collapse behavior of compacted clays by suction-controlled triaxial tests. ASTM Geotechnical Testing Journal 27 (4), 362–370.

Sun, D.A., Matsuoka, H., Yao, Y.P., Ichihara, W., 2000. An elastoplastic model for unsaturated soil in three-dimensional stresses. Soils and Foundations 40 (3), 17–28.

Tamagnini, R., 2004. An extended Cam-clay model for unsaturated soils with hydraulic hysteresis. Geotechnique 54 (3), 223–228.

Vaunat, J., Romero, E., Jommi, C., 2000. An elastoplastic hydro-mechanical model for unsaturated soils. In: Tarantino, A., Mancuso, C. (Eds.), Experimental Evidence and Theoretical Approaches in Unsaturated Soils, pp. 121–138.

Wheeler, S.J., Sivakumar, V., 1995. An elasto-plastic critical state framework for unsaturated soil. Geotechnique 45 (1), 35–53.

Wheeler, S.J., Sharma, R.S., Buisson, M.S.R., 2003. Coupling of hydraulic hysteresis and stress–strain behaviour in unsaturated soils. Geotechnique 53 (1), 41–54.